Scripta Materialia 156 (2018) 32–36

Contents lists available at ScienceDirect

Scripta Materialia

journal homepage: www.elsevier.com/locate/scriptamat

Regular article

Electrical properties, defect chemistry and local lattice relaxation in Nb_2O_5 modified $0.94(Na_{0.5}Bi_{0.5})TiO_3$–$0.06BaTiO_3$ ferroelectrics

Haiwu Zhang [a,*], Hong Yan [b], Xiaobing Li [b], Haosu Luo [b,*]

[a] Institute of Physical Chemistry, RWTH Aachen University, 52056 Aachen, Germany
[b] Key Laboratory of Inorganic Functional Materials and Devices, Shanghai Institute of Ceramics, Chinese Academy of Sciences, 215 Chengbei Road, Jiading, Shanghai 201800, China

ARTICLE INFO

Article history:
Received 25 May 2018
Accepted 3 July 2018
Available online xxxx

Keywords:
Ferroelectricity
Perovskite
Defects
Simulations

ABSTRACT

Single crystals of x at.% Nb + $0.94(Na_{0.5}Bi_{0.5})TiO_3$–$0.06BaTiO_3$ (x%-Nb:NBT-6BT, x = 0.12, 0.23, and 0.48) show improved ferroelectric and piezoelectric properties. In particular, the large piezoelectric constant (d_{33} = 532 pC/N) and high field-induced strains (S_{max} = 0.57%) in 0.23%-Nb:NBT-6BT single crystal demonstrate its promising application potential. The underlying mechanisms were investigated directively by atomistic scale simulations. We found that, Nb^{5+} cations prefer to substitute Ti^{4+} cations on *B*-site and will first fill up the oxygen vacancies generated due to the loss of Bi_2O_3 and/or Na_2O. Higher concentration of Nb_2O_5, however, will be compensated by Ti and/or Bi vacancies. The ions positions surrounding the defect center(s) were identified.

$(Na_{0.5}Bi_{0.5})TiO_3$ (NBT)-based ferroelectrics display exceptional piezoelectric properties and have captured widespread interest [1–3]. The chemically different Bi^{3+}/Na^{+} cations at *A*-site lead to complex local disorder, which inhibits the development of long-range ferroelectric order and results in the nonpolar average structure around MPB in solid solutions of $(Na_{0.5}Bi_{0.5})TiO_3$-$xBaTiO_3$ (NBT-xBT) and $(Na_{0.5}Bi_{0.5})TiO_3$-$x(K_{0.5}Bi_{0.5})TiO_3$ (NBT-xKBT) [4, 5]. However, when an external field (*E*) is applied along $\langle 100\rangle_{pc}$, the coherent lengths of the in-phase tilted regions ($a^0a^0c^+$, Glazer notation [6]) increase and phase switching from pseudocubic to tetragonal occurs. On the contrary, the coherent lengths anti-phase tilted regions ($a^-a^-a^-$) increase and an induced transition from pseudocubic to rhombohedral structures was observed for $E//\langle 111\rangle_{pc}$ [7]. These phase transformation processes generate large strains suitable for actuator applications [8]. Therefore, the piezoelectric response can be effectively tuned via chemical and/or microstructure modifications, as they can effectively modify the free energies of spontaneous and poled states.

Acceptor doping in general decreases the permittivity and piezoelectric constant, giving rise to ferroelectric "hardening effect" [9, 10]. The underlying mechanism is that the acceptor dopants form defect associations with the charge compensating oxygen vacancies, as has been found in Mn^{2+}, Cu^{2+} or Fe^{3+} doped NBT-based ferroelectrics [11–13]. The aligning of the dipoles generates an *internal bias field*, which increase the volume fraction of in-phase tilted regions and therefore promote the phase transformation from pseudocubic to tetragonal upon the application of external electrical fields. [14,15] Alternatively, donor doping increases the dielectric permittivity, piezoelectric coupling and mechanical compliance, leading to the ferroelectric "softening behavior" [9,16]. Recently, it has been found that 0.5–1 at.% Nb doping switches the conduction mechanism from oxygen-ions in undoped NBT to electronic (band gap) conduction, with the activation energy (E_a) increases from lower than 0.9 eV to higher than 1.5 eV [17, 18]. On the other hand, Zuo et al. found that the incorporation of 1 mol% Ta^{5+} enhances the field-induced strains of NBT-6BT ceramics effectively from ~0.3 to ~0.4% [19]. Furthermore, remarkably enhanced normalized field-induced strain (S_{max}/E_{max}) i.e., from 238 to 641 pm/V, was observed in the Nb^{5+}-doped NBT-18KBT ceramics [20]. These results are reminiscent the ultrahigh field-induced strains in (K, Na)NbO_3 (KNN) modified NBT-6BT [21,22].

Nevertheless, the underlying mechanisms for the improved electrical performance in donor (Nb^{5+}/Ta^{5+}) doped NBT are still not well understood. This is because the charge compensation may be realized by the formation of V_{Na}', V_{Bi}''' and/or V_{Ti}'''', which can be difficult to probe by experimental alone. Besides, the diffraction studies have encountered difficulties in identifying the local lattice relaxations around charged defects, as these techniques focus on the long-range average structures. Atomistic scale simulations are highly informative in investigating the defect properties, as well as precise identification and visualization of ion positions surrounding the defect, as have been well demonstrated in NBT, $BaTiO_3$ and other perovskite oxides [23–26]. Such mechanistic details are crucial for rational materials design for desired properties.

In this work, the ferroelectric, dielectric and piezoelectric properties of x at.% Nb + $0.94(Na_{0.5}Bi_{0.5})TiO_3$–$0.06BaTiO_3$ (x%-Nb:NBT-6BT, x = 0.12, 0.23, and 0.48) single crystals were studied systematically. The defect chemistry and lattice relaxation around the defect functional

---

[*] Corresponding authors.
E-mail addresses: zhw3789@sina.com (H. Zhang), hsluo@mail.sic.ac.cn (H. Luo).

https://doi.org/10.1016/j.scriptamat.2018.07.004
1359-6462/

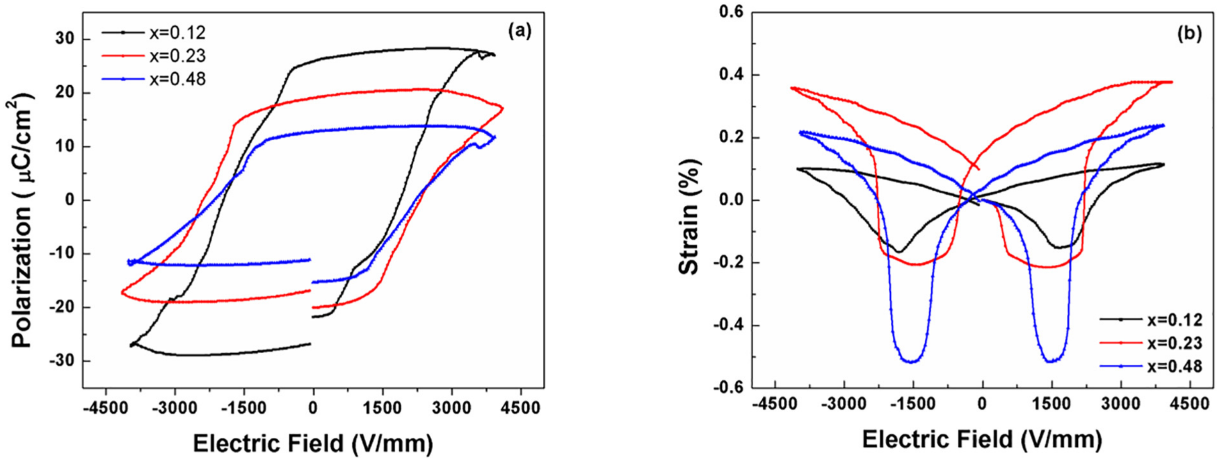

Fig. 1. (a) Polarization hysteresis (*P-E*); (b) bipolar strain curves (*S-E*) for x%-Nb:NBBT5 single crystals, under a maximum dc electric field of $E = 4$ kV/mm.

centers were investigated directively by atomistic scale simulations. The mechanisms for the enhanced ferroelectric and piezoelectric performances were discussed in detail.

The x%-Nb:NBT-6BT ($x = 0.12$, 0.23 and 0.48) single crystals were grown using a top-seeded solution growth method. The as-grown single crystals were cut along the pseudocubic (0 0 1)/(1 0 0)/(0 1 0) planes with dimensions of $5 \times 5 \times 0.5$ mm^3. Gold electrodes were sputtered on the two main faces of the samples. The polarization (*P-E*) and strain (*S-E*) hysteresis loops were measured using a ferroelectric test system (aixACCT TF-analyzer 1000). The temperature dependent dielectric properties were measured by an Agilent 4294 impedance analyzer. The piezoelectric constant (d_{33}) was measured by a quasi-static d_{33} meter of Berlincourt type at approximately 55 Hz.

Lattice minimization simulations and defect calculations were performed with the GULP code [27, 28]. The ionic interactions are described using pairwise potentials (Born models), which include a long-range Coulombic interaction between each pair of ions *i* and *j*, and a short-range Buckingham term to model overlap repulsions and van der Waals forces [29]. The short-range interactions are specified in the Buckingham form:

$$V_{ij}(r) = A_{ij}\ \exp\left(-r/\rho_{ij}\right) - C_{ij}/r^6 \tag{1}$$

where A_{ij}, ρ_{ij} and C_{ij} are the potential parameters and r is the interatomic separation. The potential parameters for lattice ions were transferred directly from our previous study on NBT (supplementary material, S1) [23], while the potential parameters for Nb^{5+}–O^{2-} were taken from G. C. Mather et al. in a study of $LaNbO_4$ [30].

An important feature is the treatment of lattice relaxation around the defect site(s). The perfect lattice was partitioned into inner and outer spherical regions centered on an individual defect or defect cluster two regions using the Mott-Littleton approach. The ions in a spherical inner region surrounding the defect are relaxed explicitly, whereas the remainder of the crystal, where the defect forces are relatively weak, were treated by more approximate quasicontinuum methods. In this way, local relaxation is effectively modelled and the crystal is not considered simply as a rigid lattice [31]. More details about the simulations can be found in comprehensive reviews given in elsewhere [32].

Fig. 1a shows the polarization hysteresis (*P-E*) for x%-Nb:NBT-6BT single crystals, in which well saturated *P-E* loops typical for ferroelectrics can be observed. With increasing Nb^{5+} doping concentration, the remnant polarization (P_r) decreases drastically from 25.8 to 19.1 and then to 12.7 μC/cm^2, while the coercive field (E_c) increases initially from 1.9 to 2.3 but decreases subsequently to 2.2 kV/mm in 0.12-, 0.23- and 0.48%-Nb:NBT-6BT single crystals, respectively. The former suggests that the field-induced ferroelectric order is destabilized and the degree of the ergodic relaxor pseudocubic state at zero field is increased, while the later indicates that the energy that needed for inducing the phase transformation is not much affected by this chemical modification [21, 33]. This is further confirmed by the bipolar strain curves (*S-E*) measurements, as shown in Fig. 1b. The 0.12%-Nb:NBT-6BT single crystal shows a typical butterfly-shaped strain hysteresis with a total field-induced strain S_{total} of 0.12%. The presence of negative strain S_{neg} indicates a drastic deviation from the typical ferroelectric behavior. This is because the presence of negative strain is closely related to the domain backswitching process on the removal of the external electrical field [34]. Further increasing the Nb^{5+} doping level to 0.48%, both of the negative strain (S_{neg}) and the total field-induced strain (S_{total}) increase dramatically and reach to the maximum values, i.e., 0.46% and 0.76%, respectively.

The electrical parameters of x%-Nb:NBT-6BT single crystals were compared with PZT ceramics are summarized in Table 1. The Nb^{5+} doping enhances the ε_r dramatically from 1100 in pure NBT-6BT to 1423 and 1438 in 0.12%- and 0.23%-Nb:NBT-6BT single crystals, respectively. However, the loss factor tanδ decrease from 2.7% in pure NBT-6BT to 2.3 and 2.6

Table 1
Electrical properties of NBT-BT single crystals as compared to PZT ceramics and other NBT-based ceramics.

Materials	ε_r	*tan*δ (%)	d_{33} (pC/N)	P_r (μC/cm^2)	E_c (kV/mm)	S_{max} (%)	Ref.
Hard PZT, PZT8[a]	1000	0.4	225	~20	~2.2	–	[38, 39]
Soft PZT, PZT-5H[a]	3400	2.0	590	~32	0.6–0.8	–	[38, 39]
NBT-6BT-2KNN[a]	2320	6.2	30	16	1.3	0.45	[21]
Pure NBT-5BT	1100	2.7	420	11.8	2.2	0.12	[13]
0.10%-Fe:NBT-6BT	988	1.5	478	48.3	2.7	1.08	[13]
0.12%-Nb:NBT-6BT	1423	2.3	497	25.8	1.9	0.28	This work
0.23%-Nb:NBT-6BT	1438	2.6	532	19.1	2.3	0.57	This work
0.48%-Nb:NBT-6BT	1293	3.7	386	12.7	2.2	0.76	This work

[a] Ferroelectric ceramics.